1-24-2015

Electrochemical Capture of CO_2 from Natural Gas using a High-Temperature Ceramic-Carbonate Membrane

Jingjing Tong
University of South Carolina - Columbia, tongj2@mailbox.sc.edu

Lingling Zhan

Jie Fang
University of South Carolina - Columbia, jief@email.sc.edu

Minfang Han

Kevin Huang
University of South Carolina - Columbia, huang46@cec.sc.edu

Publication Info

Published in *Journal of The Electrochemical Society*, Volume 162, Issue 43, 2015, pages E43-E46.

Electrochemical Capture of CO_2 from Natural Gas Using a High-Temperature Ceramic-Carbonate Membrane

Jingjing Tong,[a,b] Lingling Zhang,[b] Jie Fang,[b] Minfang Han,[a,c,z] and Kevin Huang[b,*,z]

[a]*School of Chemical & Environmental Engineering, China University of Mining & Technology, Beijing 100083, People's Republic of China*
[b]*Department of Mechanical Engineering, University of South Carolina, Columbia, South Carolina 29201, USA*
[c]*Department of Thermal Engineering, Tsinghua University, Beijing 100084, People's Republic of China*

This study reports the first investigation of using a ceramic-carbonate dual-phase membrane to electrochemically separate CO_2 from a simulated natural gas. The CO_2 permeation flux density was systematically studied as a function of temperature, CO_2 partial pressure and time. As expected, the flux density was observed to increase with temperature and CO_2 partial pressure. Long-term stability test showed that flux density experienced an initial performance-improving "break-in" period followed by a slow decay. Post-test microstructural analysis suggested that a gradual loss of carbonate during the test could be the cause of the flux-time behavior observed.
 [DOI: 10.1149/2.0481504jes] All rights reserved.

Manuscript submitted November 17, 2014; revised manuscript received January 7, 2015. Published January 24, 2015.

Natural gas is a cleaner burning and flexible alternative to other fossil fuels, and is widely used in power generation, residential, industrial, and transportation sectors.[1,2] Sources of natural gas include conventional onshore and offshore wells and unconventional wells that rely on stimulation technologies to enhance natural gas recovery in the reservoir. Examples of the latter include hydraulic fracturing in shale and water removing in coal bed methane (CBM) wells.[3,4]

The composition of natural gas varies considerably with sources, and even within a source.[5,6] Other than minor amounts of H_2S, H_2O, N_2, He and VOC (volatile organic compounds), CO_2 concentration in a natural gas can vary from 0 to 70%, see Table I. As an acidic gas, CO_2 must be removed prior to transportation in order to protect pipelines. During the removal process, avoiding accidental CH_4 release to the atmosphere is also important since CH_4 is a heat-trapping gas 86 times more powerful than CO_2. Therefore, a safe, efficient and low-cost separation process for CO_2 removal from raw natural gas is technologically and environmentally important. The conventional means of removing CO_2 from a CO_2/CH_4 mixture is based on reversible sorbent/solvent adsorption/absorption processes. Pressure swing adsorption (PSA) using zeolite,[12] metal organic framework (MOF)[13–15] and carbon nanotube[16] are some examples of sorbents used to separate CO_2 from CH_4. Amine-based liquids such as MEA or MDEA[17,18] are examples of solvents employed to capture CO_2 from CH_4, but often with high energy penalty and CH_4 loss.

Recently, organic and inorganic membranes have received much attention as an effective means of separating CO_2 from CH_4.[19–24] For instance, Peters and co-workers utilized the PVAm/PVA membrane to remove CO_2 from CH_4. The CO_2 permeance reached 3.7×10^{-8} $mol{\cdot}s^{-1}{\cdot}m^{-2}{\cdot}Pa^{-1}$ with a selectivity of 35–40.[25] Xie and co-workers studied the alumina-supported cobalt-adeninate MOF membranes for CO_2/CH_4 separation, and achieved a high CO_2 permeance 4.55×10^{-6} $mol{\cdot}s^{-1}{\cdot}m^{-2}{\cdot}Pa^{-1}$ but with a low selectivity of 3.2.[22] Venna and Carreon further reported a high CO_2 permeance of 2.4×10^{-5} $mol{\cdot}s^{-1}{\cdot}m^{-2}{\cdot}Pa^{-1}$ under a pressure differential of 40 KPa using a zeolite imidazolate framework (ZIF) membrane, but with a selectivity of 5.1.[26] As well documented in the literature, the trade-off between permeability and selectivity (or so called "Robeson Upper Bound") is a major barrier for the aforementioned membranes to overcome.[27,28] Furthermore, the requirement for high-pressure feed and low operating-temperature makes the organic membranes only suitable for high-pressure and low-temperature CO_2 separation from streams such as pre-combustion products where pressure of 25–30 bar and temperature of <50°C are typically present. For post-combustion carbon capture, where near ambient-pressure and high-temperature CO_2-containing streams are present, the membrane technology is less advantageous compared to its solvent and sorbent rivals.

Very recently, we as well as other groups have developed a new type of membranes based on electrochemical principles. The membrane is composed of an oxide-ion conducting ceramic and carbonate-ion conducting carbonate phase, forming a mixed oxide-ion and carbon-ion conductor (MOCC). The membranes have been demonstrated with high-flux and high-selectivity in separating CO_2 from a mixture of CO_2/N_2 (for example, CO_2 flux = 0.13 $ml{\cdot}cm^{-2}$ min^{-1} with a membrane thickness of 1.32 mm at 650°C) and $CO_2/H_2/N_2$ (for example, CO_2 flux = 1.84 $ml{\cdot}cm^{-2}$ min^{-1} with a membrane thickness of 1.2 mm at 700°C).[29–34] Here we report that MOCC membranes can also separate CO_2 from CH_4 with high-flux and selectivity even under the ambient pressure. The oxide-ion conducting ceramic matrix used in this study was a samarium doped ceria (SDC), within which a carbonate-ion conducting eutectic mixture of Li_2CO_3-Na_2CO_3 was held. A schematic illustrating the overall CO_2 permeation process though a MOCC membrane with CH_4/CO_2 as the feeding gas and helium as the sweeping gas is shown in Fig. 1. The driving force for the CO_2 separation is the chemical potential (partial pressure) of CO_2 existing across the MOCC membrane. At the CH_4-CO_2/MOCC interface, CO_2 reacts with O^{2-} to form CO_3^{2-}. The formed CO_3^{2-} then transports though the molten carbonate phase toward the MOCC/Helium interface where a reverse reaction occurs to release CO_2 and O^{2-};[29–31] O^{2-} then migrates in an opposite direction through the oxide-ion matrix to charge compensate the flux of CO_3^{2-}. Evidently, only CO_2 can transport across the membrane as long as there is no physical leakage, yielding exclusive selectivity for CO_2 separation. Therefore, the "Robeson Upper Boundary" is no longer applicable to electrochemical membranes like MOCC.

Table I. Variations of CO_2 concentration in natural gas.[7–11]

Natural gas type	CO_2 concentration (%)
Ordinary natural gas	0–70
Shale gas	0–12
Gas hydrates	0–1
Coal bed	30–55
Biogas from organic waste	30–45
Biogas form landfill	30–60
Biogas from sewage digester	30–45

*Electrochemical Society Active Member.
[z]E-mail: huang46@cec.sc.edu; hanminfang@sina.com

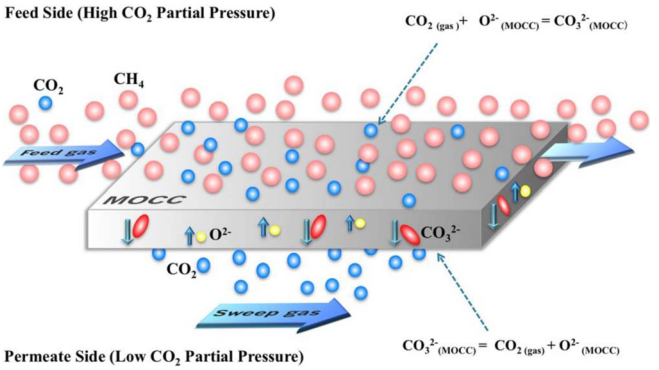

Figure 1. Schematic illustration of working principle of MOCC membranes for CO_2/CH_4 separation.

Experimental

Fabrication of MOCC membranes.— The fabrication of MOCC membranes includes two steps. The first step is the making of porous ceramic SDC matrix. To maximize the homogeneity and minimize the size of the pores, a "co-precipitation" and "sacrificial template" technique was employed.[29] The porosity of the SDC matrix fabricated for this study was controlled to be 0.4. Thus fabricated porous matrix was then infiltrated at 650°C with eutectic molten carbonates of Li_2CO_3 and Na_2CO_3 in a molar ratio of 52:48, forming a dense MOCC membrane.[30] Details about the procedure can be found in our previous work.[30,31]

CO_2 permeation measurement.— The CO_2 permeation measurements on MOCC membranes were performed using a homemade test station and established test protocol, both of which can also be found in our previous work.[29–31] The button cell membranes used to evaluate the permeation flux have a diameter of 17 mm, thickness of 1.2 mm, and effective area of 0.921 cm^2. The effect of temperature on CO_2 flux was studied in the temperature range of 600 -700°C with a simulated natural gas containing 75%CH_4, 15%CO_2 and 10%N_2 as the feeding gas; N_2 was used as the tracer gas to indicate and quantify any leakage. The effect of CO_2 partial pressure on CO_2 flux was investigated by varying mass flow rates of the constituents in the feeding gas. In doing so, the flow rates of CO_2 was varied from 15–50 ml·min^{-1} while N_2 flow rate was fixed at 20 ml·min^{-1}; CH_4 served as the balance to keep the total flow rate at 120 ml·min^{-1}. The actual flow rates of CO_2, CH_4 and N_2 used for this study are listed in Table II. While changing the partial pressure of oxygen in the feed gas can impact on the resultant CO_2 flux as was previously demonstrated [30], the variation of CH_4 concentrations would not affect the partial pressure of oxygen in the feed gas as both CH_4 and N_2 are considered inert. The long-term stability of MOCC in a simulated natural gas containing 15% CO_2 was also evaluated at 650°C. The microstructure of the membrane after the long-term operation was further examined by scanning electron microscope (SEM) to understand the root cause of the degradation.

Results and Discussion

The effect of temperature.— The Arrhenius plot of CO_2 flux density, J_{CO2}, measured with a simulated natural gas containing 15%CO_2 as the feeding gas is shown in Fig. 2. As expected, J_{CO2} increases with temperature, indicating that the permeation of CO_2 is a thermally activated process. The slope of the straight-line (ln (J_{CO2}) vs 1000/T) yields an activation energy of E_a = 48.86 kJ mol^{-1}. This value is lower than that of SDC,[32] a rate-limiting phase previously identified for the CO_2 transport in MOCC.[30] One possible reason for the lowered E_a is the electronic conduction induced by the reduction of Ce^{4+} at low partial pressure of oxygen (Po_2) exposed to the membrane. Overall, at 700°C, J_{CO2} reaches 0.11 ml·min^{-1}·cm^{-2}, a moderately high flux-density for the membrane thickness and operating temperature tested.

Table II. Mass flow rates (mL·min^{-1}) of CO_2, CH_4 and N_2 used to make different CO_2 concentrations of the feeding gas.

	Gas1	Gas2	Gas3	Gas4	Gas5	Gas6	Gas7	Gas8
CO_2	15	20	25	30	35	40	45	50
CH_4	85	80	75	70	65	60	55	50
N_2	20	20	20	20	20	20	20	20

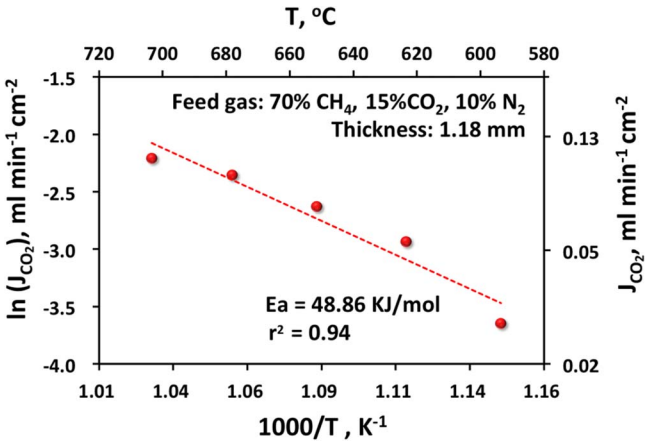

Figure 2. Arrhenius plots of CO_2 flux density in a simulated natural gas containing 15% CO_2.

The effect of CO_2 partial pressure.— For the same sample, the J_{CO2} was also measured as a function of the gradient of CO_2 partial pressure at 650°C; the result is shown in Fig. 3. A linear relationship is clearly observed, suggesting that a modified Wagner equation previously established for the CO_2 transport could also be applicable to this study:[30]

$$J_{CO_2} \approx -\frac{\varepsilon}{\tau}\frac{RT}{4F^2L}(1-\varphi)(\sigma_{O^{2-}})ln\frac{P''_{CO_2}}{P'_{CO_2}}$$

Here ε and τ are the porosity and tortuosity of the porous SDC matrix, respectively; φ is the volume fraction of carbonate phase; $\sigma_{O^{2-}}$ is the conductivity of O^{2-}, P'_{CO_2} is the higher CO_2 partial pressure at

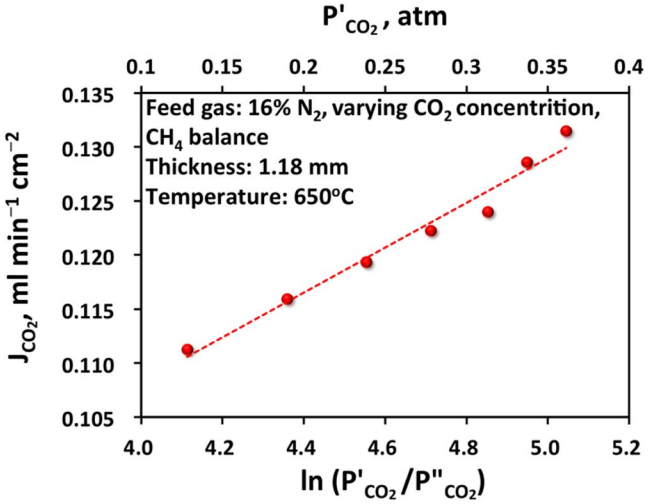

Figure 3. CO_2 flux density as function of logarithm of CO_2 partial pressure across the membrane.

Table III. Performance comparison among different membranes for CO_2/CH_4 separation.

Membranes	Permeance × Thickness mol·s^{-1}·m^{-1}·Pa^{-1}	Selectivity (CO_2/CH_4)	Ref.
PVAm/PVA	7.4×10^{-13}	35–45	25
Cobalt-adeninate MOF	$2.2–5.9 \times 10^{-11}$	3.2–3.8	22
ZIF	$1.4–2.2 \times 10^{-10}$	4–7	26
MOCC	$6.4–7.7 \times 10^{-11}$	>100	This study

the feeding side and P''_{CO_2} is the lower CO_2 partial pressure at the sweeping side; L is the thickness of the membrane; F, R and T have their usual meanings.

From the slope $\sigma_{O^{2-}}$ is estimated to be 41.5 S/m according to $-\frac{\varepsilon}{\tau}\frac{RT}{4F^2L}(1-\varphi)(\sigma_{O^{2-}})$ with $\varepsilon \approx \varphi = 0.4$, $\tau \approx 11.3$,[30] L = 0.00118 m, R = 8.314 J·mol^{-1}·K^{-1} and F = 96485 C·mol^{-1}; this value is much greater than $\sigma_{O^{2-}}$ (923 K) = 3.1 S·m^{-1} reported for air.[34,35] The higher $\sigma_{O^{2-}}$ may be attributed to the presence of electron conduction in SDC when exposed to low-Po_2 atmosphere or simply oversimplification of the Wagner equation.

The highest CO_2 flux reached 0.13 ml·min^{-1}·cm^{-2} at 650°C and P'_{CO2} = 0.375 atm. It is worth mentioning that J_{CO2} shown in Fig. 3 is higher than in Fig. 2, e.g., 0.11 ml·min^{-1}·cm^{-2} at 650°C in Fig. 3 vs 0.11 ml·min^{-1}·cm^{-2} at 700°C in Fig. 2. We attribute it to the performance improving "break-in" behavior occurring during the flux-temperature measurement period that produced Fig. 2. The following long-term stability study further supports this assertion by showing an early-stage performance improvement "break-in" behavior.

The performance of MOCC is also compared in Table III with other types of membranes. Note that the flux-density obtained in this study has to be converted to permeance with the consideration of membrane thickness and pressure differential in order to compare with other membranes on the same basis. The selectivity of CO_2/CH_4 was determined from the concentration of N_2 in the sweeping gas leaked through the membrane. Within the N_2 concentration (<0.03%) detected in the sweeping helium, the selectivity of CO_2 is calculated to be >100. Evidently, the electrochemical MOCC membrane is advantageous over other size-exclusion membranes in permeance and selectivity, and is virtually unlimited by the "Robeson Upper Bound".[27,28]

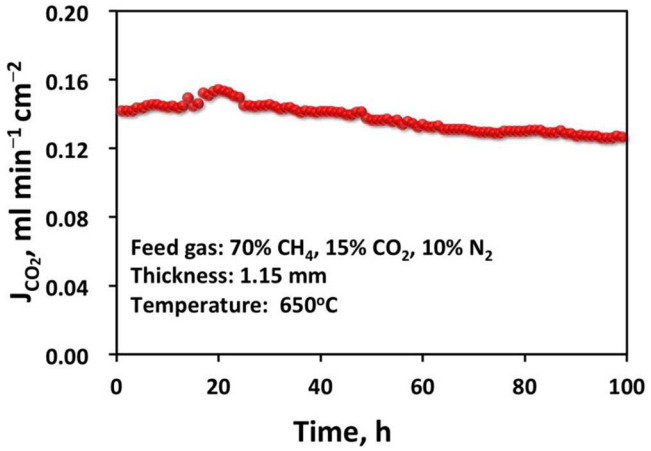

Figure 4. CO_2 flux stability measured with a simulated natural gas containing 15%CO_2 at 650°C.

Long-term flux stability.— The long-term stability of the membrane with a simulated natural gas containing 15% CO_2 as the feeding gas is shown in Fig. 4. Note that this was a new membrane performing better than the one producing Figs. 2 and 3. The better performance is likely attributed to a thinner membrane and better control of membrane synthesis. In addition, an increase in J_{CO2} during the first 20 hours is noted, followed by a slow degradation. The initial flux increase was probably due to a gradual loss of carbonate, which may make the effective thickness of the membrane gradually smaller with time.[29–31] Overall, the degradation rate is relatively small; the flux density remains >0.12 ml·min^{-1}·cm^{-2} even after 100 hours. Our most recent study has shown that the loss of carbonate can be mitigated by modifying the surface of oxide matrix with Al_2O_3 as the latter has a full wettability with molten carbonates and thus increases membrane's ability to immobilize molten carbonates inside the porous ceramic skeleton.[33,36]

The microstructures of the membrane at various locations before and after the long-term test are shown in Fig. 5. In particular, the

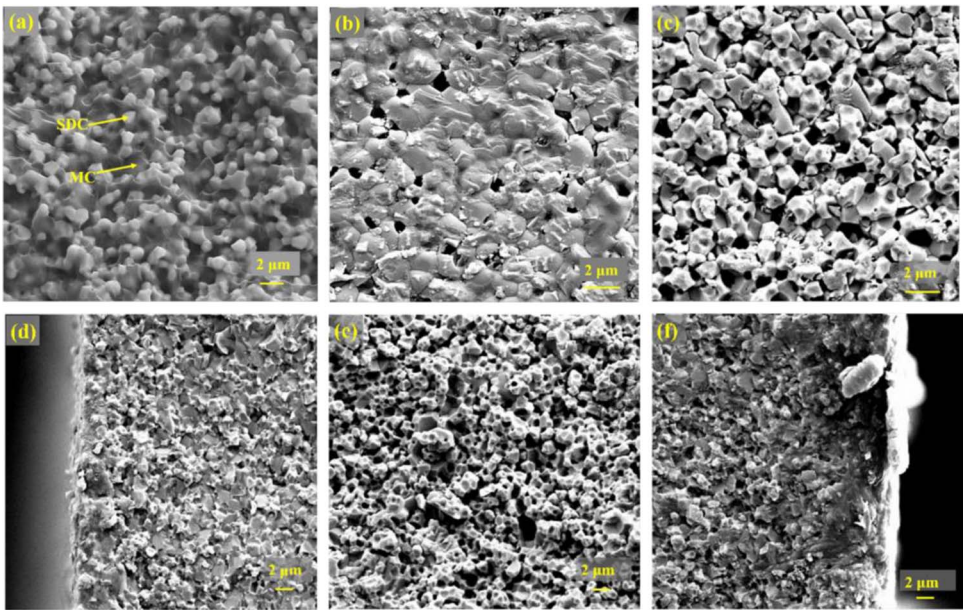

Figure 5. SEM images of membrane (a) cross sectional view before test; (b)-(f) are after 100-h test: (b) sweep side of the membrane; (c) feed side of the membrane; (d) cross section near the sweep side; (e) center of the cross section; (f) cross section near the feed side.

surface and sub-surface regions of the sweeping-gas side located at the bottom of the cell, Fig. 5b and 5d, are heavily covered by carbonate, implying a downward movement of carbonate during the test. The surface and sub-surface regions of the feeding-gas side located at the top of the cell are shown in Fig. 5c and 5f with porosity and partially filled carbonate, respectively, indirectly supporting the downward movement of carbonate. What is a surprise is the large amount of porosity observed in the mid-section of the membrane, Fig. 5e. Such as a "sandwich-like" structure seems to suggest that carbonate at the mid-section moved faster than the top layer toward the sweeping-gas side during operation. In future research, we will further investigate fundamentals of the phenomenon and develop approaches to mitigating the movement of carbonate within ceramic porous structures.

Conclusions

The electrochemical SDC-carbonate MOCC membrane has been successfully demonstrated for CO_2 separation from a simulated natural gas containing 12.5 to 37.5% CO_2 with high flux density and selectivity. The CO_2 flux density increases with temperature and CO_2 concentration in the feeding gas. The maximum flux density of CO_2 reaches 0.133 $ml{\cdot}min^{-1}{\cdot}cm^{-2}$ at 650°C and CO_2 concentration of 37.5%. Furthermore, the flux remains > 0.12 $ml{\cdot}min^{-1}{\cdot}cm^{-2}$ during a 100-h stability test at the same temperature. The gradual loss of carbonate during the operation is thought to be the reason for the initial increase and later decrease in flux density.

Acknowledgment

Financial supports from NSF (CBET-1340269, CBET-1401280), U. S. Army Research Office (W911NF-10-R-006 and W911NF-13-1-0158) are greatly appreciated. JT and MH specially thank for support from China Scholarship Council (CSC).

References

1. D. M. Kargbo, R. G. Wilhelm, and D. J. Campbell, *Environ. Sci. Technol.* **44**, 5679 (2010).
2. T. E. Rufford, S. Smart, G. C. Y. Watson, B. F. Graham, J. Boxall, J. C. Diniz da Costa, and E. F. May, *J. Pet. Sci. Eng.* **94–95**, 123 (2012).
3. D. Rahm, *Energy Policy*, **39**, 2974 (2011).
4. J. T. Rutledge and W. S. Phillips, *Geophysics*, **68**, 441 (2003).
5. E. L. First, M. M. Faruque Hasan, and C. A. Floudas, *AIChE*, **60**, 1767 (2014).
6. Y. Bae, K. L. Mulfort, H. Frost, P. Ryan, S. Punnathanam, L. J. Broadbelt, J. T. Hupp, and R. Q. Snurr, *Langmuir*, **24**, 8592 (2008).
7. Y. Liu and J. Wilcox, *Environ. Sci. Technol.* **45**, 809 (2011).
8. R. H. Weiland and N. A. Hatcher, *Hydrocarbon Process.* January, 45 (2012).
9. Y. F. Makogon, *J. Nat. Gas Sci. Eng.* **2**, 49 (2010).
10. S. Rasi, A. Veijanen, and J. Rintala, *Energy*, **32**, 1375 (2007).
11. K. A. Kvenvolden, *Rev. Geophys.* **31**, 173 (1993).
12. S. Cavenati, C. A. Grande, and A. E. Rodrigues, *J. Chem. Eng. Data*, **49**, 1095 (2004).
13. J. Li, J. Yang, L. Li, and J. Li, *J. Energy Chem.* **23**, 453 (2014).
14. R. Krishna, *Microporous Mesoporous Mater*. **156**, 217 (2012).
15. P. Mishra, S. Mekala, F. Dreisbach, B. Mandal, and S. Gumma, *Sep. Purif. Technol.* **94**, 124 (2012).
16. S. Furmaniak, A. P. Terzyk, P. Kowalczyk, K. Kaneko, and P. A. Gauden, *Phys. Chem. Chem. Phys.* **15**, 16468 (2013).
17. G. T. Rochelle, *Science*, **325**, 1652 (2009).
18. R. Sanz, G. Calleja, A. Arencibia, and E. S. Sanz-Perez, *J. Mater. Chem. A*, **1**, 1956 (2013).
19. W. J. Koros and R. Mahajan, *J. Membr. Sci.* **175**, 181 (2000).
20. S. Zhao, Z. Wang, Z. Qiao, X. Wei, C. Zhang, J. Wang, and S. Wang, *J. Mater. Chem. A*, **1**, 246 (2013).
21. B. Xue, L. Gao, H. Jiang, Z. Geng, S. Guan, Y. Wang, Z. Liu, and L. Jiang, *J. Mater. Chem. A*, **1**, 8097 (2013).
22. Z. Xie, T. Li, N. L. Rosi, and M. Carreon, *J. Mater. Chem. A*, **2**, 1239 (2014).
23. R. W. Baker and K. Lokhandwala, *Ind. Eng. Chem. Res.* **47**, 2109 (2008).
24. A. W. Thornton, D. Dubbeldam, M. S. Liu, B. P. Ladewing, A. J. Hill, and M. R. Hill, *Energy Environ. Sci.* **5**, 7637 (2012).
25. Lars Peters, A. Hussain, M. Follmann, T. Melin, and M. B. Hagg, *Chem. Eng. J.* **172**, 952 (2011).
26. S. R. Venna and M. A. Carreon, *J. Am. Chem. Soc.* **132**, 76 (2010).
27. L. M. Robeson, *Curr. Opin. Solid State Mater. Sci.* **4**, 549 (1999).
28. L. M. Robeson, *J. Membr. Sci.* **320**, 390 (2008).
29. L. Zhang, X. Li, S. Wang, K. G. Romito, and K. Huang, *Electrochem. Comm.* **13**, 554 (2011).
30. L. Zhang, N. Xu, X. Li, S. Wang, and K. Huang, *Energy Environ. Sci.* **5**, 8310 (2012).
31. L. Zhang, Z. Mao, D. Thomason, S. Wang, and K. Huang, *J. Am. Ceram. Soc.* **95**, 1832 (2012).
32. X. L. Dong, J. Ortiz-Landeros, and Y. S. Lin, *Chem. Comm.* **49**, 9654 (2013).
33. T. T. Norton, B. Lu, and Y. S. Lin, *J. Membr, Sci.* **467**, 244 (2014).
34. J. L. Wade, C. Lee, A. C. West, and K. S. Lackner, *J. Membr. Sci.* **369**, 20 (2011).
35. T. Mori, Y. Wang, J. Drennan, G. Auchterlonie, J. G. Li, and T. Ikegami, *Solid State Ionics*, **175**, 641 (2004).
36. L. Zhang, Y. Gong, J. Yaggie, S. Wang, K. Romito, and K Huang, *J. Membr. Sci.* **453**, 36 (2014).
37. F. Gaillard, M. Malki, G. Iacono-Mariziano, M. Pichavant, and B. Scaillet, *Science*, **322**, 1363 (2008).
38. B. Steele, *Solid State Ionics*, **129**, 95, (2000).
39. L. Zhang, J. Tong, Y. Gong, M. Han, and S. Wang, *J. Membr. Sci.* **468**, 373 (2014).